Evolutionary convergence in lignin-degrading enzymes

Iván Ayuso-Fernández[a], Francisco J. Ruiz-Dueñas[a,1], and Angel T. Martínez[a,1]

[a]Centro de Investigaciones Biológicas, Consejo Superior de Investigaciones Científicas, E-28040 Madrid, Spain

Edited by C. Kevin Boyce, Stanford University, Stanford, CA, and accepted by Editorial Board Member David Jablonski May 7, 2018 (received for review February 12, 2018)

The resurrection of ancestral enzymes of now-extinct organisms (paleogenetics) is a developing field that allows the study of evolutionary hypotheses otherwise impossible to be tested. In the present study, we target fungal peroxidases that play a key role in lignin degradation, an essential process in the carbon cycle and often a limiting step in biobased industries. Ligninolytic peroxidases are secreted by wood-rotting fungi, the origin of which was recently established in the Carboniferous period associated with the appearance of these enzymes. These first peroxidases were not able to degrade lignin directly and used diffusible metal cations to attack its phenolic moiety. The phylogenetic analysis of the peroxidases of Polyporales, the order in which most extant wood-rotting fungi are included, suggests that later in evolution these enzymes would have acquired the ability to degrade nonphenolic lignin using a tryptophanyl radical interacting with the bulky polymer at the surface of the enzyme. Here, we track this powerful strategy for lignin degradation as a phenotypic trait in fungi and show that it is not an isolated event in the evolution of Polyporales. Using ancestral enzyme resurrection, we study the molecular changes that led to the appearance of the same surface oxidation site in two distant peroxidase lineages. By characterization of the resurrected enzymes, we demonstrate convergent evolution at the amino acid level during the evolution of these fungi and track the different changes leading to phylogenetically distant ligninolytic peroxidases from ancestors lacking the ability to degrade nonphenolic lignin.

convergent evolution | ancestral enzyme resurrection | lignin | Polyporales | fungal peroxidases

Degradation of lignin is essential for carbon recycling in land ecosystems and often represents a key step for the use of biomass in the industry (1). The main organisms that are able to mineralize lignin are white-rot fungi, using an array of oxidative enzymes (2). Three class II peroxidases of the peroxidase-catalase superfamily (3) are involved in the initial attack on lignin: (*i*) lignin peroxidases (LiP), which are able to oxidize its major nonphenolic moiety (4); (*ii*) manganese peroxidases (MnP) including short and long MnPs with slightly different properties (5) that oxidize Mn^{2+} to Mn^{3+}, the diffusible chelates of which oxidize the minor phenolic moiety of lignin (6); and (*iii*) versatile peroxidases (VP), which combine the catalytic properties of LiP, MnP, and plant peroxidases (the latter oxidizing phenolic monolignols) (7, 8). Also, white-rot fungi produce generic peroxidases (GP), catalytically similar to plant peroxidases. The above four peroxidase types have been characterized, and their structural and kinetic properties are well known (9). Thereby, they can oxidize substrates at three sites: (*i*) the main heme access channel, where low redox-potential compounds are oxidized (in all of them); (*ii*) a Mn^{2+}-oxidizing site, formed by three acidic residues near one of the heme propionates (10) (in MnP and VP); and (*iii*) a surface tryptophan (11, 12) that is able to oxidize lignin directly (13, 14) via an aminoacyl radical and long-range electron transfer to heme (15) (in VP and LiP).

In past years, there has been an increasing interest in the evolution of wood-degrading organisms. The origin of lignin degradation by fungi, associated with the appearance of the first ligninolytic peroxidases, has been estimated to have occurred during the Carboniferous period, playing a role in the decline of coal accumulation near the end of the Permo-Carboniferous (16). However, geoclimatic factors would have also significantly contributed to coal formation under ever-wet tropical conditions, and its decline could also be related to climatic shifts toward drier conditions (17, 18). Then, the expansion and diversification of genes encoding ligninolytic peroxidases occurred leading to the families existing today, as shown by genomic and evolutionary studies (16, 19, 20). The diversity and evolution of these enzymes have been studied particularly in the order Polyporales, where the lignicolous habitat is largely predominant, resulting in the most efficient ligninolytic enzymes. Recent studies included first analyses of the appearance and disappearance of relevant catalytic sites (20) and later sequence reconstruction, heterologous expression ("resurrection"), and experimental characterization of some ancestral enzymes (21). The evolutionary analysis of peroxidases shows phylogenetically distant enzymes (corresponding to the above LiP and VP types) that would be a priori able to oxidize nonphenolic lignin at the exposed catalytic tryptophan (11–15, 22). To determine if the LiP/VP distribution in the peroxidase phylogeny is due to duplication of an ancestor and maintenance of function or to a convergent process, we first performed phylogenetic analyses and ancestral sequence reconstruction of Polyporales peroxidases from sequenced genomes. This choice should enable a precise description on the evolution of ligninolytic enzymes within this order, although the reconstruction of enzymes predating Polyporales could be partially biased. Then we compared in the laboratory the previously described line leading to extant LiP (21) with a new independent evolutionary line leading

Significance

We analyze the molecular mechanisms that led to the rise of a powerful strategy for lignin degradation (i.e., the formation of a solvent-exposed tryptophanyl radical capable of oxidizing the bulky lignin polymer) as a convergent trait in different species of fungi (order Polyporales). We use ancestral sequence reconstruction and enzyme resurrection to obtain the ancestors of the two extant types of ligninolytic peroxidases—lignin peroxidase (LiP) and versatile peroxidase (VP)—and compare their predicted molecular structures and catalytic properties after resurrection. The results presented demonstrate convergent evolution in distant LiP and VP lineages with the exposed tryptophan residue appearing twice, as two independent events, following different molecular changes.

Author contributions: F.J.R.-D. and A.T.M. designed research; I.A.-F. performed research; I.A.-F., F.J.R.-D., and A.T.M. analyzed data; and I.A.-F., F.J.R.-D., and A.T.M. wrote the paper.

The authors declare no conflict of interest.

This article is a PNAS Direct Submission. C.K.B. is a guest editor invited by the Editorial Board.

[1]To whom correspondence may be addressed. Email: fjruiz@cib.csic.es or atmartinez@cib.csic.es.

This article contains supporting information online at www.pnas.org/lookup/suppl/doi:10.1073/pnas.1802555115/-/DCSupplemental.

to extant VP, and established their convergent evolution using empirical analyses of resurrected enzymes.

Results

Ancestral Sequences of Polyporales Peroxidases. For reconstructing the ancestral sequences leading to the extant lignin-degrading peroxidases in Polyporales, we built a phylogenetic tree with RAxML (Fig. 1) after manual annotation of the complete set of peroxidase sequences (a total of 113) in the sequenced genomes of *Bjerkandera adusta*, *Ceriporiopsis subvermispora*, *Dichomitus squalens*, *Fomitopsis pinicola*, *Ganoderma* sp., *Phlebia brevispora*, *Phanerochaete chrysosporium*, *Postia placenta*, *Trametes versicolor*, and *Wolfiporia cocos*. For the present analysis, the tree was divided into (*i*) clade A containing GPs; (*ii*) clade B, including two subclades of short MnPs and VPs; (*iii*) clade C formed exclusively of long MnPs; and (*iv*) clade D containing short MnPs and some VPs, together with the large LiP subclade. B and D are the only clades that contain enzymes that a priori would oxidize nonphenolic lignin due to the presence of the exposed catalytic tryptophan. To explain the presence of this residue in two phylogenetically different peroxidase clades, horizontal gene transfer between lines D and B was first ruled out, since no similarities were detected between the flanking regions of genes encoding clade D LiPs and clade B VPs. Double-gene transfer (from outside Polyporales) was also rejected since BLAST search of both extant genes on the National Center for Biotechnology Information database show sequence identities only with genes of Polyporales peroxidases. Therefore, duplication of the gene of an ancestral peroxidase containing the tryptophan and its differentiation in lines B and D or convergent evolution were considered.

To decide between these two alternative hypotheses, we performed ancestral sequence reconstruction with PAML. The average posterior probability, for the predicted amino acids in each reconstructed sequence, always was >0.95, except for the most ancestral reconstructed sequence (*SI Appendix*, Fig. S1). More importantly, no ambiguity was observed for the positions of the catalytic tryptophan, the Mn^{2+} oxidation site, or other residues relevant for catalysis described below. Then we selected six ancestral enzymes and two lignin-degrading extant peroxidases—the highly expressed *T. versicolor* VP2 (23) and the well-known *P. chrysosporium* LiPA (LiPH8) (4)—for heterologous expression and comparative characterization. The eight sequences define two well-separated evolutionary lines leading to the above extant ligninolytic peroxidases (TV-VP2 and PC-LiPA). Both pathways begin with the Common ancestor of Polyporales peroxidases (CaPo), which is the precursor of gene lineages leading to clade B VP (blue line in Fig. 1) and clade D LiP (red line in Fig. 1). In this way, CaPo gave rise to the Common ancestors of clades D (CaD) and B (CaB). Therefore, the main evolutionary change is the independent and parallel appearance of the surface tryptophan in two ancestral states of both lines: Ancestral VP of line B (AVP-b) and Ancestral VP of line D (AVP-d). After this event, there are no significant modifications in the evolution of peroxidases in line B up to the extant enzyme (TV-VP2). However, in line D evolution, AVP-d lost its Mn^{2+} oxidation site, giving rise to the first LiP of the phylogeny (Ancestral LiP, ALiP) that later evolves into extant LiPs of clade D (including PC-LiPA). The molecular mechanisms that lead to the emergence of the surface tryptophan are different in both lines, as described below (and indicated on the ancestral nodes in Fig. 1).

Structural Comparison of Two Peroxidase Lineages. The amino acid sequences of the ancestors and the two extant peroxidases show 56–87% identity (*SI Appendix*, Table S1). Their multiple alignment (*SI Appendix*, Fig. S2) reveals that there have not been strong modifications in the conserved regions during evolution, beyond the changes in the oxidation sites that we describe below.

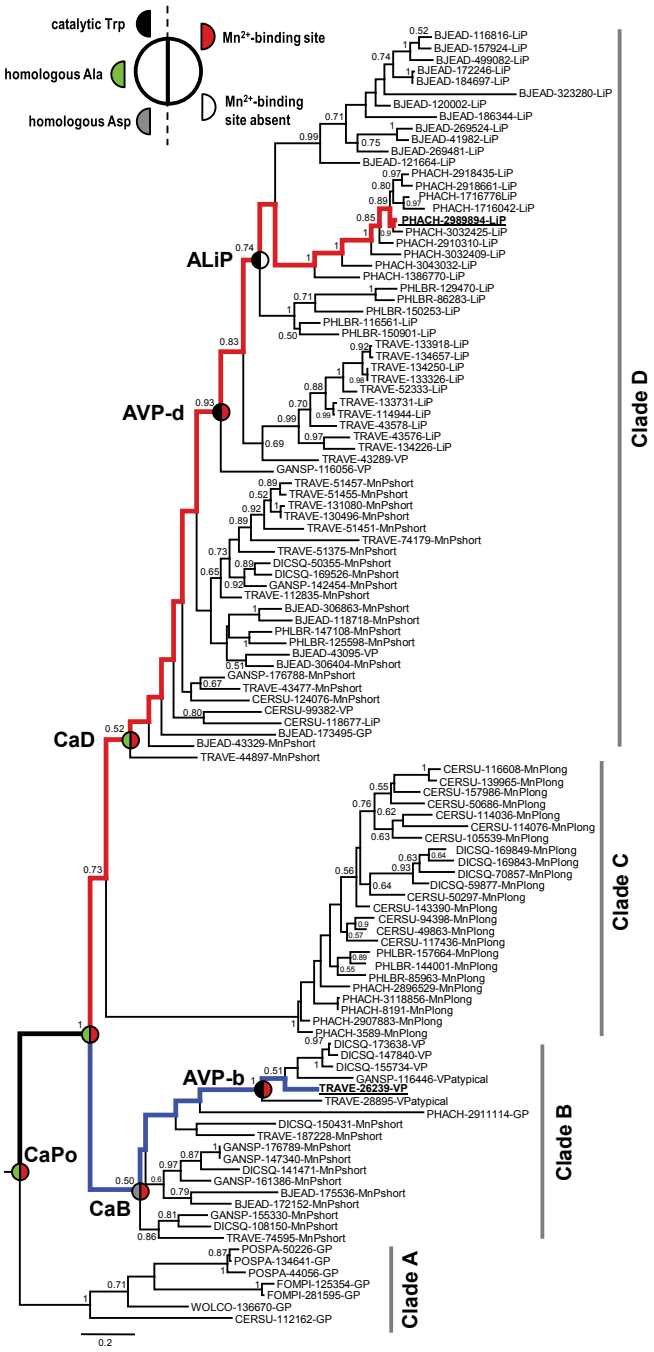

Fig. 1. Phylogenetic tree of 113 peroxidases from 10 Polyporales genomes (sequences in Dataset S1; bootstrap values ≥0.5 are indicated). Clades A–D are shown. The paths to the extant LiPA of *P. chrysosporium* (JGI ID# 2989894) and VP2 of *T. versicolor* (JGI ID# 26239) are shown in red and blue, respectively. Also, the milestones in these evolutionary lines (CaPo for both lines; CaD, AVP-d, and ALiP in red line; and CaB and AVP-b in blue line) are marked. The circles show the characteristics of the oxidation sites present in each of these nodes (*Left*: catalytic tryptophan and homologous residues; *Right*: Mn^{2+} oxidation site). The sequence labels start with the species code (BJEAD, *B. adusta*; CERSU, *C. subvermispora*; DICSQ, *D. squalens*; FOMPI, *F. pinicola*; GANSP, *Ganoderma* sp; PHACH, *P. chrysosporium*; PHLBR, *P. brevispora*; POSPL, *P. placenta*; TRAVE, *T. versicolor*; and WOLCO, *W. cocos*) followed by the JGI ID# and the peroxidase type, including GP, LiP, MnP-short, MnP-long, VP, and VP-atypical.

Moreover, the molecular models (Fig. 2) show that the overall structure, with 12 helices, two structural Ca^{2+} ions, and four disulfide bonds, is maintained through time. A more detailed

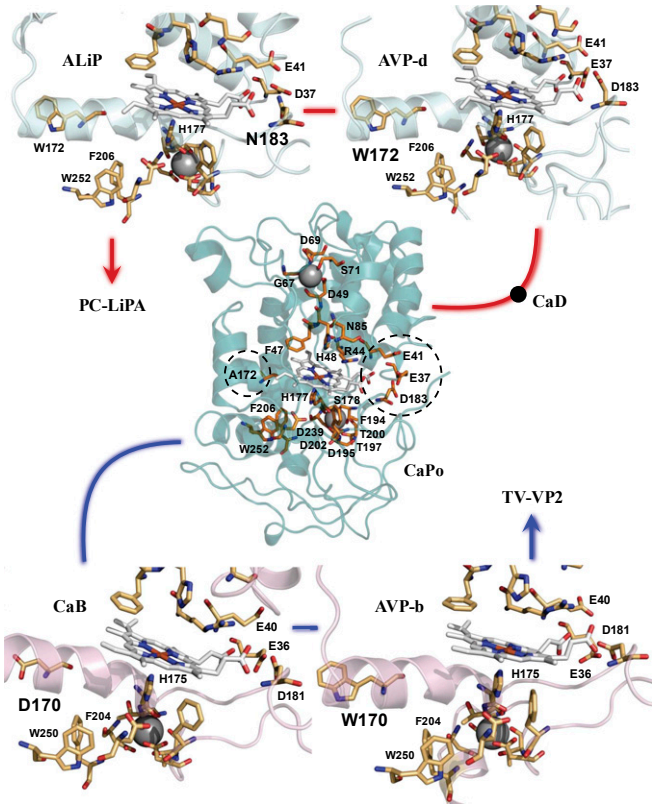

Fig. 2. Molecular model of ancestral CaPo and its main structural changes in evolution. The most relevant amino acids of the common ancestor (CaPo) are labeled, and only the main changes in the oxidation sites are represented for the other peroxidases (two structural Ca^{2+} ions are shown as gray spheres). The Mn^{2+}-binding site, formed by three acidic residues, and Ala172, homologous to catalytic tryptophan, are circled in CaPo. Red line: changes in line D evolution, with the appearance of Trp172 in AVP-d and loss of the Mn^{2+}-binding site due to the Asn183 appearance in ALiP. Blue line: changes in line B evolution, with the appearance of Asp170 in CaB that later changed to Trp170 for lignin oxidation by AVP-b. Aromatic residues (Phe206 and Trp252 in CaPo) involved in long-range electron transfer from the exposed tryptophan are conserved from the first ancestor.

analysis shows that all of the enzymes have a well-defined heme pocket with a proximal His177 coordinating the $Fe^{3+}$of the heme, Asp239, and Phe194 at one side of the heme (numbers referred to CaPo and line D) and a distal His48, Arg44 (two residues that participate in reaction with H_2O_2), Asn85, and Phe47 at the opposite side (His47, Arg43, Asn84, and Phe46 in line B). The Ca^{2+} ions would be similarly coordinated in all of the enzymes with small differences that would not affect the anchorage of the cation.

The main differences are related to the oxidation sites that these peroxidases have. These sites are identified in all of the ancestors, and we tracked their change as they evolved. The Mn^{2+}-binding site is defined by three acidic residues that already appear in CaPo (Glu37, Glu41, and Asp183) and are maintained both in line B until the extant TV-VP2 (Glu36, Glu40 and Asp181) and in line D until AVP-d. In this line, the Mn^{2+}-binding site is lost in ALiP (Asp183 becomes Asn183: Fig. 2, red line) and remains absent in all extant LiPs. Note that clade C, the sister clade of clade D (Fig. 1), evolved maintaining the Mn^{2+} oxidation site.

The site for direct oxidation of lignin is located in a surface tryptophan, and electrons are transferred to the heme following a preferred route involving buried Trp251 and Phe205 in PC-LiPA (15). Analysis of the homologous oxidation site in CaPo reveals that the ancestral surface residue was Ala172, while the amino acids of the route are present since the origin (Trp252 and Phe206 in CaPo) and conserved through evolution (Fig. 2). Therefore, although the scaffold for electron transfer is present, the absence of the required exposed tryptophan would have impeded for the most ancestral enzymes the direct oxidation of lignin.

The appearance of the catalytic tryptophan in line D occurs in AVP-d (Trp172, Figs. 1 and 2, red line), the first enzyme of this line that would be able to modify lignin directly. After AVP-d, both ALiP and PC-LiPA maintain the surface tryptophan. The study of the same oxidation site in line B shows that, in the common ancestor of this clade (CaB), Ala172 became Asp170, which later changed to Trp170 in AVP-b (and is maintained in TV-VP2, Figs. 1 and 2, blue line). Thus, the same oxidation site appears twice in evolution, and, interestingly, different sequences of changes led to the same catalytic amino acid in parallel processes. Therefore, this event is defined as a convergent trait in lignin degradation by fungal peroxidases. To confirm the ability to oxidize lignin model compounds, and compare the catalytic properties in both convergent lines, we resurrected the described ancestral enzymes as reported below.

Reaction Kinetics and Convergent Evolution of Ancestral Peroxidases. The selected enzymes from the two evolutionary lines (Fig. 1) were resurrected by *Escherichia coli* expression of the synthesized genes, in vitro-activated and purified, and their catalytic properties were analyzed using five substrates, which define the different oxidation sites that these peroxidases can have. Veratryl alcohol (VA) was used as a model for nonphenolic lignin, while 2,6-dimethoxyphenol (DMP) was tested representing the minor phenolic moiety of lignin. The oxidation of Mn^{2+} was also analyzed, since Mn^{3+} oxidizes phenolic lignin. Finally, the oxidation of two dyes, often used as high (Reactive Black 5, RB5) and low (2,2′-azinobis[3-ethylbenzothiazoline-6-sulfonate], ABTS) redox-potential peroxidase substrates, was also assayed. As we described above, the sites for the oxidation of Mn^{2+} and high-redox-potential substrates (VA and RB5) are well defined in the structure of these enzymes. Moreover, low redox-potential substrates (DMP and ABTS) can be oxidized, with high efficiency, at the same tryptophan responsible for oxidation of high-redox-potential substrates and, with low efficiency, at one of the heme-access channels, resulting in biphasic kinetics, as shown for some extant peroxidases (24).

Catalytic constant (k_{cat}) and affinity constant (K_m) were calculated for all of the resurrected and extant peroxidases (*SI Appendix*, Table S2), but what is clear with evolution is the change in the catalytic efficiency (k_{cat}/K_m) with time (Fig. 3, *Upper* bars). CaPo, the common ancestor of both lines, is an enzyme that can oxidize low-redox-potential substrates in the low-efficiency site, but also Mn^{2+} at the specific binding site. After that, the respective common ancestors of each line (CaB and CaD) are almost identical in their catalytic properties: both are able to oxidize low-redox-potential substrates (in their low-efficiency sites) and Mn^{2+}. Interestingly, the same trend is observed in both ancestors: they reduce the catalytic efficiency oxidizing ABTS and DMP while the efficiency oxidizing Mn^{2+} is improved. From this point on, the trends in lines B and D are different, taking into account the nature of their catalytic sites and the reactions that they perform. While the efficiency oxidizing Mn^{2+} decreases in AVP-b (blue line in Fig. 3), AVP-d attains the highest value among all enzymes analyzed here (red line in Fig. 3). Later, in the evolution of clade B, there are no changes in the oxidation of the cation (in TV-VP2) while in clade D the Mn^{2+} oxidation site/activity is lost.

The nonphenolic lignin model substrate VA begins to be oxidized in parallel in both lines, as a convergent trait in AVP-b and AVP-d, coinciding with the appearance of the catalytic tryptophan. However, the evolution of the catalytic efficiency differs. While in line D the efficiency oxidizing VA increases in ALiP and is maximal in PC-LiPA (red line in Fig. 3), it is maintained at low levels in TV-VP2 of clade B (blue line in Fig. 3). Interestingly, the

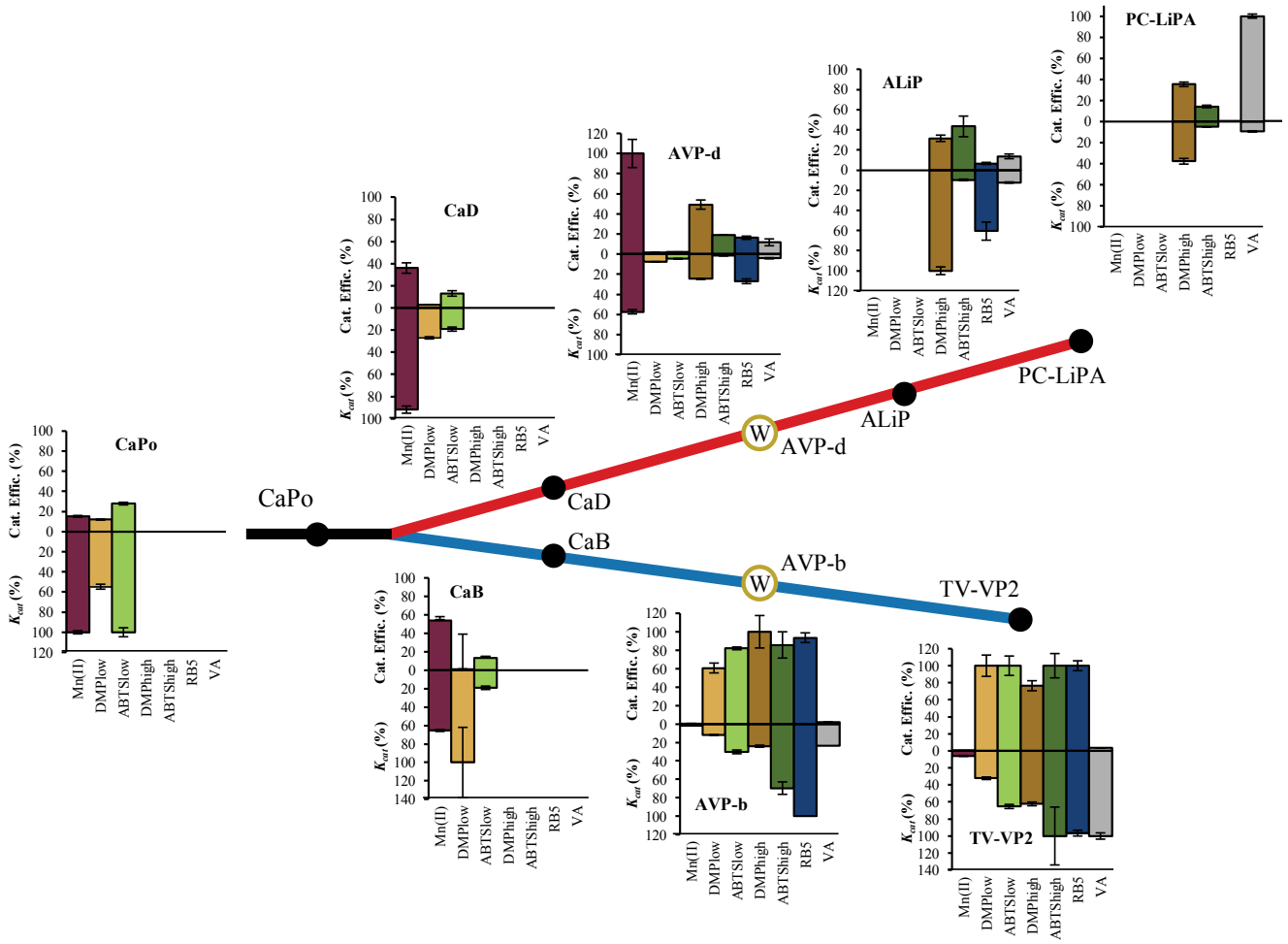

Fig. 3. Evolution of catalytic properties in the D (red line) and B (blue line) evolutionary pathways. Changes of catalytic efficiency (*Upper* bars) and k_{cat} (*Lower* bars) are shown for oxidation of Mn^{2+} (purple); DMP at low- and high-efficiency sites (light and dark brown, respectively); ABTS at low- and high-efficiency sites (light and dark green, respectively); RB5 (blue); and VA (gray) (means and 95% confidence limits). For each substrate, the maximum value was taken as 100% and referred to that for the other enzymes (see *SI Appendix*, Table S2 for absolute values). The circled W marks the point when the catalytic tryptophan appeared for the first time, and black circles represent the other nodes analyzed.

k_{cat} for VA is always high in line B, with the TV-VP2 value being eightfold the observed for ALiP (the highest in line D) (Fig. 3, *Lower* bars). The main reason for a low catalytic efficiency of the two VPs in line B is the high K_m that they have (*SI Appendix*, Table S2)—three to four magnitude orders greater than observed for the enzymes of line D. One explanation for differences in the activity of peroxidases in lines B and D is the different charge distribution in the surface environment of the catalytic tryptophan. As shown in Fig. 4, the tryptophan (or homologous residue) environment in line D is progressively more acidic while a similar tendency was not observed in line B. A more electronegative environment will promote stabilization of positively charged compounds (such as the VA cation radical) and, more importantly, will increase the oxidizing power of the catalytic radical.

Stability Comparison in the Two Peroxidase Lineages. We analyzed the pH stability of the ancestors and extant enzymes in the evolutionary lines B (*SI Appendix*, Fig. S3) and D (*SI Appendix*, Fig. S4) by measuring the residual activity after a 4-h incubation at 25 °C in the pH 2–10 range. Overall, the stability at pH 4–6 is higher in the ancestors of clade B while the ancestors of clade D are more stable at a pH > 6 (where, in contrast, CaB, AVP-b, and TV-VP2 are inactivated). More interestingly, the stability at pH 3 (where ligninolysis takes place in nature) strongly increases during the last evolution steps (Fig. 5*A*), either in parallel with the appearance of the catalytic tryptophan (line D) or after its appearance (line B).

Thermal denaturation was studied by circular dichroism (T_m values) and residual activity measurement (T_{50} values) of peroxidases in lines B (*SI Appendix*, Fig. S5) and D (*SI Appendix*, Fig. S6). The melting profiles parallel the changes observed in activity in all cases and tended to decrease during evolution (line D), although all of the T_{50} values were in the 55–65 °C range (Fig. 5*B*). The main change was observed when the Mn^{2+}-binding site disappeared in line D, diminishing the thermal stability (in ALiP and PC-LIPA). The higher stability in line B, and in more ancestral line D, enzymes is in agreement with the Mn^{2+} contribution to cofactor binding.

Discussion

The main evidence about the basidiomycete enzymes involved in lignin degradation comes from the genomic information available in the past years. Every study shows the presence of LiP, MnP, or VP genes in the sequenced genomes of all typical white-rot (lignin-degrading) fungi and their absence from all typical brown-rot (cellulose-degrading) fungi and some poor wood rotters (16, 19, 20, 25).

Here, we analyzed the appearance and subsequent evolution of phylogenetically distant LiP- and VP-type genes within the evolution of Polyporales, resulting in the most efficient ligninolytic

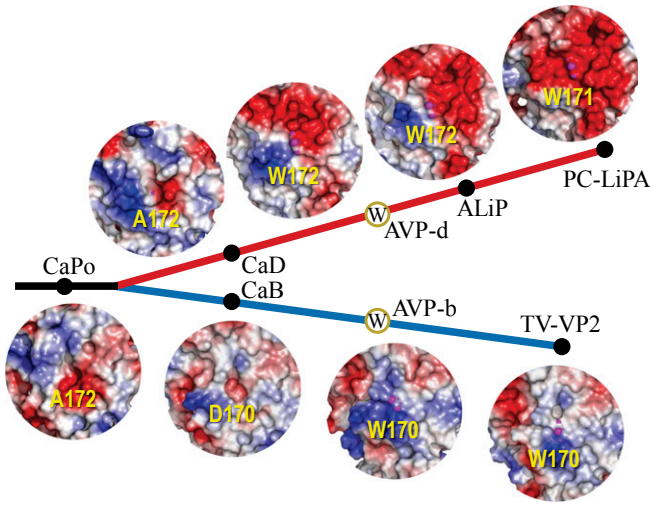

Fig. 4. Changes in the electrostatic surface of the environment of the catalytic tryptophan and homologous residues (pink spheres in the center) in peroxidase evolution. In line B to TV-VP2 (blue line), the changes are more subtle, but in line D to PC-LiPA (red line), a clear increase in the negative charge (red) happened with time.

enzymes. Although the first class II fungal peroxidase(s) most probably appeared by horizontal transfer of a prokaryotic peroxidase (such as cytochrome *c* peroxidase) gene from an ancestral organelle (26), no evidence for subsequent horizontal transfer in Polyporales was obtained by BLAST searches (27) in agreement with the very rare nature of such events in basidiomycetes (28). However, evolutionary clues of the presence of the same lignin-degradation mechanism in distant Polyporales peroxidases could be obtained by ancestral sequence reconstruction and characterization of the resurrected enzymes.

For sequence reconstruction, we used maximum likelihood (ML) methods that have some advantages over other approaches (29). To deal with the inherent limitations and uncertainties in ancestral reconstructions (30), (*i*) we used the best data available, i.e., all of the class II peroxidase genes in 10 Polyporales genomes after their careful revision and manual annotation (20), and (*ii*) we verified that no ambiguity exists in the amino acids forming the different oxidation sites (31). The reconstructed sequences revealed that the appearance of the surface tryptophan abstracting electrons from lignin (13, 14) was not an isolated event in the evolution in Polyporales. Moreover, the biochemical characterization of the resurrected ancestral peroxidases enabled us to confirm their predicted new catalytic properties and revealed how they progressively changed in the two evolutionary lines analyzed, as discussed below.

First, the experimental characterization of the resurrected enzymes showed the evolvability (32) of fungal peroxidases in the exploration of new mechanisms to modify lignin at different points of their phylogeny. The common ancestor of Polyporales peroxidases (CaPo) was most probably a short MnP that used Mn^{3+} to attack the phenolic moiety of lignin and other phenolic molecules, acting synergistically with secreted oxidases and intracellular oxidoreductases. By comparison with analyses with a broader sampling of genomes (although including fewer Polyporales species) (16), CaPo would correspond with the common ancestor of all Agaricomycetes class II ligninolytic peroxidases, not just those of Polyporales, and is estimated to have existed roughly 400 Mya (results from molecular clock analyses with fossil calibration). Note that the common ancestor of Polyporales fungi, appearing at the early Cretaceous, would already have several (3–13) peroxidase genes (ligninolytic and GP included) (16). Therefore, the higher expansion and specialization of peroxidases would postdate the Carboniferous, although the fungal capacity to degrade lignin would occur earlier using ancestral peroxidases (like CaPo) oxidizing the minor phenolic moiety of lignin and phenolic ancestral polymers. After CaPo, the common ancestors of clades D (CaD) and B (CaB) would have almost identical properties (both in activity and stability). This includes an increase in the efficiency of oxidizing Mn^{2+} that reveals a similar initial degradative strategy in the two branches, using Mn^{3+} chelates. Reconstruction of these old peroxidases would be more uncertain than for the three more recent ancestors, which already appeared within Polyporales. The oxidation site for high-redox-potential substrates appeared in both lines, and VA (the laboratory model substrate for lignin degradation studies) was oxidized by the resurrected enzymes. MnPs would be efficient degrading ancestral phenolic polymers and phenolic lignin in plants, but MnP's action on nonphenolic lignin would require the concerted action of LiPs and VPs. In this way, ancient fungi would incorporate a powerful tool into their degradative machinery.

After the catalytic tryptophan appearance, we observed an increase in the peroxidase efficiency oxidizing VA in both branches, but the kinetic parameters and the evolution of other oxidation sites were different. Evolution in line D focused on a better degradation of lignin by removing other oxidation sites (at the expense of the stability conferred by the Mn^{2+}-binding site) and maintaining the surface tryptophan, with a progressively more acidic environment (that increases the tryptophanyl radical reactivity). However, VPs in clade B maintain both oxidation sites. Although VPs could be seen as mere evolutionary intermediates, as found in line D, a significant improvement in the oxidation of VA was observed in both branches after the appearance of the catalytic tryptophan. In addition to the changes in the architecture and activity of the oxidation sites, we also observed an increase with evolution in the peroxidase stability under the acidic conditions that characterize the hyphal microenvironment where ligninolysis takes place in nature (33). In clade D, the appearance of the new oxidation site comes along with a huge increase in acidic stability, but in clade B this stability is acquired later. Either way, there is a clear improvement toward the stabilization at pH 3, where the oxidizing power of these enzymes is the highest (34, 35).

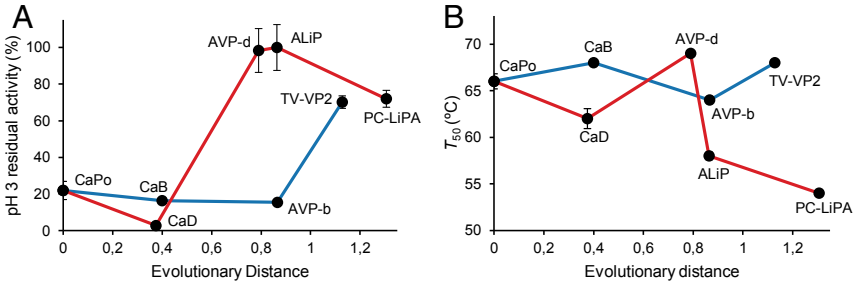

Fig. 5. The pH and thermal stabilities in the D (red line) and B (blue line) evolutionary pathways. (*A*) Changes in residual activity after incubation at pH 3. (*B*) Changes in T_{50}. Means and 95% confidence limits are shown.

The above evolutionary trend, which results in more efficient oxidation of lignin, was most probably related to changes in plant cell wall and tissue anatomy. Despite the evolutionary history of lignins remaining unclear, there have been significant changes in their composition and structure including convergent evolution between different vascular plants (36, 37). Angiosperms are the plants with the more complex lignin (38, 39), including a higher relative abundance of syringyl units with the C_3 and C_5 positions of the aromatic ring blocked by methoxyls, compared with most gymnosperms, that results in a predominance of nonphenolic (C_4-etherified) units (40). The angiosperm appearance (140–250 Mya) (41) roughly corresponds with the age of the two most recent ancestors of major clades B and D of ligninolytic peroxidases in Polyporales (~200 Mya) that subsequently incorporated the exposed catalytic tryptophan almost at the same time (16). This evolutionary event resulted in the most efficient peroxidases that oxidize nonphenolic lignin by long-range electron transfer from the protein surface, as shown using methylated lignin (13). Interestingly, a similar electron transfer mechanism has been developed by plant peroxidases involved in lignin polymerization, with the appearance of an enzyme being able to oxidize the bulkier (dimethoxylated) sinapyl alcohol monolignol characterizing angiosperm lignin at a surface aromatic residue (42).

Materials and Methods

The 113 sequences of class II peroxidases in the genomes of *B. adusta*, *C. subvermispora*, *D. squalens*, *F. pinicola*, *Ganoderma* sp., *P. brevispora*, *P. chrysosporium*, *P. placenta*, *T. versicolor*, and *W. cocos* (Dataset S1) available at the Department of Energy Joint Genome Institute (JGI) were used in this study. ML phylogeny was constructed with RAxML (43), and PAML 4.7 (44) was used to obtain the most probable ancestral sequences that were manually corrected for insertions or deletions and synthesized for *E. coli* expression. Molecular models were obtained at the Swiss-Model server (45). The coding DNA sequences of ancestral and extant peroxidases were cloned and used to transform *E. coli*. The apoenzymes were recovered from inclusion bodies, in vitro-activated, and purified. Mn^{2+}, VA, ABTS, DMP, and RB5 were used for kinetic characterization at the optimal pH and H_2O_2 concentrations (see *SI Appendix*, Table S2 footnote *a*). For pH stability, the peroxidases were incubated at pH 2–10 for 4 h, and activity was estimated with ABTS. For thermal stability, the enzymes were incubated for 10 min at 25–85 °C (pH 5.5) to obtain T_{50} values. Circular dichroism was used to obtain T_m values. See *SI Appendix* for details.

ACKNOWLEDGMENTS. This work was supported by the IndOx (KBBE-2013-613549, https://www.indoxproject.eu) and EnzOx2 (H2020-BBI-PPP-2015-2-720297, https://www.enzox2.eu) European Union projects and the BIO2014-56388-R and BIO2017-86559-R Spanish projects. The work conducted by JGI was supported by the Office of Science of the US Department of Energy under Contract DE-AC02-05CH11231. I.A.-F. acknowledges a Spanish FPI (Formación del Personal Investigador) Fellowship.

1. Martínez AT, Ruiz-Dueñas FJ, Martínez MJ, Del Río JC, Gutiérrez A (2009) Enzymatic delignification of plant cell wall: From nature to mill. *Curr Opin Biotechnol* 20:348–357.
2. Ruiz-Dueñas FJ, Martínez AT (2009) Microbial degradation of lignin: How a bulky recalcitrant polymer is efficiently recycled in nature and how we can take advantage of this. *Microb Biotechnol* 2:164–177.
3. Zámocký M, et al. (2015) Independent evolution of four heme peroxidase superfamilies. *Arch Biochem Biophys* 574:108–119.
4. Hammel KE, Cullen D (2008) Role of fungal peroxidases in biological ligninolysis. *Curr Opin Plant Biol* 11:349–355.
5. Fernández-Fueyo E, et al. (2014) Structural implications of the C-terminal tail in the catalytic and stability properties of manganese peroxidases from ligninolytic fungi. *Acta Crystallogr D Biol Crystallogr* 70:3253–3265.
6. Gold MH, Youngs HL, Gelpke MD (2000) Manganese peroxidase. *Met Ions Biol Syst* 37:559–586.
7. Camarero S, Sarkar S, Ruiz-Dueñas FJ, Martínez MJ, Martínez AT (1999) Description of a versatile peroxidase involved in the natural degradation of lignin that has both manganese peroxidase and lignin peroxidase substrate interaction sites. *J Biol Chem* 274:10324–10330.
8. Ruiz-Dueñas FJ, Martínez MJ, Martínez AT (1999) Molecular characterization of a novel peroxidase isolated from the ligninolytic fungus *Pleurotus eryngii*. *Mol Microbiol* 31:223–235.
9. Ruiz-Dueñas FJ, Martínez AT (2010) Structural and functional features of peroxidases with a potential as industrial biocatalysts. *Biocatalysts Based on Heme Peroxidases*, eds Torres E, Ayala M (Springer, Berlin), pp 37–59.
10. Kishi K, et al. (1996) Characterization of manganese(II) binding site mutants of manganese peroxidase. *Biochemistry* 35:8986–8994.
11. Pérez-Boada M, et al. (2005) Versatile peroxidase oxidation of high redox potential aromatic compounds: Site-directed mutagenesis, spectroscopic and crystallographic investigation of three long-range electron transfer pathways. *J Mol Biol* 354:385–402.
12. Smith AT, Doyle WA, Dorlet P, Ivancich A (2009) Spectroscopic evidence for an engineered, catalytically active Trp radical that creates the unique reactivity of lignin peroxidase. *Proc Natl Acad Sci USA* 106:16084–16089.
13. Sáez-Jiménez V, et al. (2016) Role of surface tryptophan for peroxidase oxidation of nonphenolic lignin. *Biotechnol Biofuels* 9:198.
14. Sáez-Jiménez V, et al. (2015) Demonstration of lignin-to-peroxidase direct electron transfer: A transient-state kinetics, directed mutagenesis, EPR, and NMR study. *J Biol Chem* 290:23201–23213.
15. Acebes S, et al. (2017) Mapping the long-range electron transfer route in ligninolytic peroxidases. *J Phys Chem B* 121:3946–3954.
16. Floudas D, et al. (2012) The Paleozoic origin of enzymatic lignin decomposition reconstructed from 31 fungal genomes. *Science* 336:1715–1719.
17. Nelsen MP, DiMichele WA, Peters SE, Boyce CK (2016) Delayed fungal evolution did not cause the Paleozoic peak in coal production. *Proc Natl Acad Sci USA* 113:2442–2447.
18. Hibbett D, Blanchette R, Kenrick P, Mills B (2016) Climate, decay, and the death of the coal forests. *Curr Biol* 26:R563–R567.
19. Nagy LG, et al. (2016) Comparative genomics of early-diverging mushroom-forming fungi provides insights into the origins of lignocellulose decay capabilities. *Mol Biol Evol* 33:959–970.
20. Ruiz-Dueñas FJ, et al. (2013) Lignin-degrading peroxidases in Polyporales: An evolutionary survey based on 10 sequenced genomes. *Mycologia* 105:1428–1444.
21. Ayuso-Fernández I, Martínez AT, Ruiz-Dueñas FJ (2017) Experimental recreation of the evolution of lignin-degrading enzymes from the Jurassic to date. *Biotechnol Biofuels* 10:67.
22. Mester T, et al. (2001) Oxidation of a tetrameric nonphenolic lignin model compound by lignin peroxidase. *J Biol Chem* 276:22985–22990.
23. Carabajal M, et al. (2013) The secretome of *Trametes versicolor* grown on tomato juice medium and purification of the secreted oxidoreductases including a versatile peroxidase. *J Biotechnol* 168:15–23.
24. Morales M, et al. (2012) Two oxidation sites for low redox potential substrates: A directed mutagenesis, kinetic, and crystallographic study on *Pleurotus eryngii* versatile peroxidase. *J Biol Chem* 287:41053–41067.
25. Riley R, et al. (2014) Extensive sampling of basidiomycete genomes demonstrates inadequacy of the white-rot/brown-rot paradigm for wood decay fungi. *Proc Natl Acad Sci USA* 111:9923–9928.
26. Passardi F, et al. (2007) Prokaryotic origins of the non-animal peroxidase superfamily and organelle-mediated transmission to eukaryotes. *Genomics* 89:567–579.
27. Zhaxybayeva O (2009) Detection and quantitative assessment of horizontal gene transfer. *Horizontal Gene Transfer: Genomes in Flux*, eds Gogarten MB, Gogarten JP, Olendzenski LC (Humana Press, Totowa, NJ), pp 195–213.
28. Fitzpatrick DA (2012) Horizontal gene transfer in fungi. *FEMS Microbiol Lett* 329:1–8.
29. Omland KE (1999) The assumptions and challenges of ancestral state reconstructions. *Syst Biol* 48:604–611.
30. Royer-Carenzi M, Pontarotti P, Didier G (2013) Choosing the best ancestral character state reconstruction method. *Math Biosci* 242:95–109.
31. Liberles DA (2007) *Ancestral Sequence Reconstruction* (Oxford Univ Press, Oxford).
32. Colegrave N, Collins S (2008) Experimental evolution: Experimental evolution and evolvability. *Heredity (Edinb)* 100:464–470.
33. Martínez AT (2002) Molecular biology and structure-function of lignin-degrading heme peroxidases. *Enzyme Microb Technol* 30:425–444.
34. Millis CD, Cai DY, Stankovich MT, Tien M (1989) Oxidation-reduction potentials and ionization states of extracellular peroxidases from the lignin-degrading fungus *Phanerochaete chrysosporium*. *Biochemistry* 28:8484–8489.
35. Oyadomari M, Shinohara H, Johjima T, Wariishi H, Tanaka H (2003) Electrochemical characterization of lignin peroxidase from the white-rot basidiomycete *Phanerochaete chrysosporium*. *J Mol Catal B Enzym* 21:291–297.
36. Novo-Uzal E, Pomar F, Ros LVG, Espineira JM, Barcelo AR (2012) Evolutionary history of lignins. *Advances in Botanical Research (Lignins: Biosynthesis, Biodegradation and Bioengineering)* (Elsevier, Amsterdam), Vol 61, pp 311–350.
37. Weng JK, Chapple C (2010) The origin and evolution of lignin biosynthesis. *New Phytol* 187:273–285.
38. Martínez AT, et al. (2008) Monolignol acylation and lignin structure in some nonwoody plants: A 2D NMR study. *Phytochemistry* 69:2831–2843.
39. Ralph J, et al. (2004) Lignins: Natural polymers from oxidative coupling of 4-hydroxyphenylpropanoids. *Phytochem Rev* 3:29–60.
40. Camarero S, Bocchini P, Galletti GC, Martínez AT (1999) Pyrolysis-gas chromatography/mass spectrometry analysis of phenolic and etherified units in natural and industrial lignins. *Rapid Commun Mass Spectrom* 13:630–636.
41. Magallón S, Gómez-Acevedo S, Sánchez-Reyes LL, Hernández-Hernández T (2015) A metacalibrated time-tree documents the early rise of flowering plant phylogenetic diversity. *New Phytol* 207:437–453.
42. Shigeto J, Itoh Y, Tsutsumi Y, Kondo R (2012) Identification of Tyr74 and Tyr177 as substrate oxidation sites in cationic cell wall-bound peroxidase from *Populus alba* L. *FEBS J* 279:348–357.
43. Stamatakis A, Hoover P, Rougemont J (2008) A rapid bootstrap algorithm for the RAxML Web servers. *Syst Biol* 57:758–771.
44. Yang Z (2007) PAML 4: Phylogenetic analysis by maximum likelihood. *Mol Biol Evol* 24:1586–1591.
45. Biasini M, et al. (2014) SWISS-MODEL: Modelling protein tertiary and quaternary structure using evolutionary information. *Nucleic Acids Res* 42:W252–W258.

SI Appendix

Evolutionary convergence in lignin degrading enzymes

Iván Ayuso-Fernández, Francisco J. Ruiz-Dueñas and Angel T. Martínez

Centro de Investigaciones Biológicas, CSIC, Ramiro de Maeztu 9, E-28040, Madrid, Spain

The SI Appendix includes Supporting Materials and Methods, Supporting **Figs. S1-S6** and **Tables S1** and **S2** and Supporting References.

Supporting Materials and Methods

Phylogenetic analysis, ancestral enzyme reconstruction and molecular modeling. Every class-II peroxidase (113 sequences) annotated in the genomes of ten Polyporales (phylum Basidiomycota) species (namely *B. adusta*, *C. subvermispora*, *D. squalens*, *F. pinicola*, *Ganoderma* sp., *P. brevispora*, *P. chrysosporium*, *P. placenta*, *T. versicolor* and *W. cocos*, see file S1) were used in this study, being available at the DOE JGI Mycocosm portal as http://genome.jgi.doe.gov/Bjead1_1/Bjead1_1.home.html (1), http://genome.jgi.doe.gov/Cersu1/Cersu1.home.html (2), http://genome.jgi.doe.gov/Dicsq1/Dicsq1.home.html (3), http://genome.jgi.doe.gov/Fompi3/Fompi3.home.html (3), http://genome.jgi.doe.gov/Gansp1/Gansp1.home.html (1), http://genome.jgi.doe.gov/Phlbr1/Phlbr1.home.html (1), http://genome.jgi.doe.gov/Phchr2/Phchr2.home.html (4), http://genome.jgi.doe.gov/Pospl1/Pospl1.home.html (5), http://genome.jgi.doe.gov/Trave1/Trave1.home.html (3) and http://genome.jgi.doe.gov/Wolco1/Wolco1.home.html (3), respectively. BLAST (Basic Local Alignment Search Tool) was used for the search of sequences similar to line-D LiPs and line-B VPs at the NCBI databases (with Polyporales genes included/excluded).

The amino-acid sequences were aligned using MUSCLE as implemented in MEGA 7 (6). The sequences were tested using ProtTest (7) to determine the evolutionary model that best fits the data for the ML analysis among 64 empirical models of evolution. The ML phylogeny was then constructed using RAxML (8), under the Whelan and Goldman (9) model of evolution using gamma-distributed rate of heterogeneity (gamma shape with 4 rates of categories = 1.33) with empirical amino-acid frequencies and invariant sites (proportion of invariant sites = 0.073) (WAG+I+G+F).

PAML 4.7 package (10) was used to obtain the most probable sequence at each node of the phylogeny and the posterior amino-acid probability per site in each ancestor. We used the WAG model of evolution, and the previously obtained ML phylogeny and the MUSCLE alignment as inputs for the software. Both joint and marginal reconstructions were performed and the most probable sequences of the marginal reconstruction were selected and manually corrected for C-terminal and other insertions or deletions according to the sequences of the ancestor progeny. The genes were synthesized by ATG:biosynthetics (Merzhausen, Germany) using the most frequent codons for high expression in *E. coli*.

Molecular models of the predicted proteins were obtained at the Swiss-Model protein homology modeling server (11,12) using related crystal structures, selected using the GMQE parameter, as templates (PDB entries 4BM1, 3FJW, 1QPA and 1B85 corresponding to *Pleurotus ostreatus* MnP4, *Pleurotus eryngii* VPL and *P. chrysosporium* LiPD and LiPA, respectively). All protein models had great quality taking into account the Swiss-Model parameters (good QMEAN and high GMQE). The electrostatic surfaces were computed with PyMOL v1.8 (Schrödinger LLC, http://pymol.org) using default parameters.

***E. coli* expression and characterization of the resurrected enzymes.** After gene synthesis, the coding DNA sequences of the selected ancestors (CaPo, CaB, CaD, AVP-d, AVP-b and ALiP) and the extant PC-LiPA (JGI ID# 2989894) and TV-VP2 (JGI ID# 29236) were cloned into pET23b(+) (Novagen). The resulting plasmids were transformed into BL21(DE3)pLysS (ancestors and extant TV-VP2) or W3110 (PC-LiPA) as reported by Pérez-Boada et al (13). The apoenzymes accumulated in inclusion bodies and, after solubilization in 8 M urea, the *in vitro* activation conditions of the ancestral proteins and extant TV-VP2 were optimized - including 0.16 M urea, 5 mM $CaCl_2$, 15 µM hemin, 0.4 mM oxidized glutathione, 0.1 mM dithiothreitol and 0.1 mg/mL of protein in 50 mM Tris-HCl, pH 9.5 - while those reported by Doyle and Smith (14) where used for PC-LiPA. The active enzymes were purified with a Resource-Q column (GE-Healthcare) using a 0-400 mM NaCl salt gradient, 2 mL/min flow, in 10 mM sodium tartrate, pH 5.5, containing 1 mM of $CaCl_2$.

Five substrates were selected for the kinetic characterization of the resurrected peroxidases: Mn^{2+} (Mn^{3+}-tartrate complex ε_{238} 6500 $M^{-1}\cdot cm^{-1}$), VA (veratraldehyde ε_{310} 9300 $M^{-1}\cdot cm^{-1}$), ABTS (cation radical ε_{436} 29300 $M^{-1}\cdot cm^{-1}$), DMP (dimeric coerulignone ε_{469} 55000 $M^{-1}\cdot cm^{-1}$), and RB5 (ε_{598} 30000 $M^{-1}\cdot cm^{-1}$). These reactions were analyzed at 25 ºC and the optimal pH (determined using 50 mM Britton-Robinson, B&R, buffer, pH 2-10) and H_2O_2 concentration (determined using 2.5 mM ABTS as substrate) for each enzyme (see **Table S2** footnote).

To study the pH stability, the resurrected peroxidases were incubated in B&R buffer, pH 2-10, at 25 ºC for 4 h. The residual activity was estimated by the oxidation of ABTS (2.5 mM), with the activity after 1 min at pH 5.5 (25 ºC) taken as 100%. To study thermal stability, the enzymes were incubated in 10 mM acetate, pH 5.5, for 10 min in the range 25-85 ºC, to obtain the T_{50} values (i.e. the temperature at which 50% of the activity was lost after 10 min incubation). The effect of temperature on enzyme (6 µM) circular dichroism spectra was addressed studying the changes at 222 nm from 20ºC to 95ºC, 30ºC/h, using a Jasco J-815 spectropolarimeter with a 0.01 cm path length quartz cell. T_m represents the temperature at the midpoint of the unfolding transition in the thermal melting profiles.

Supporting Figures and Tables

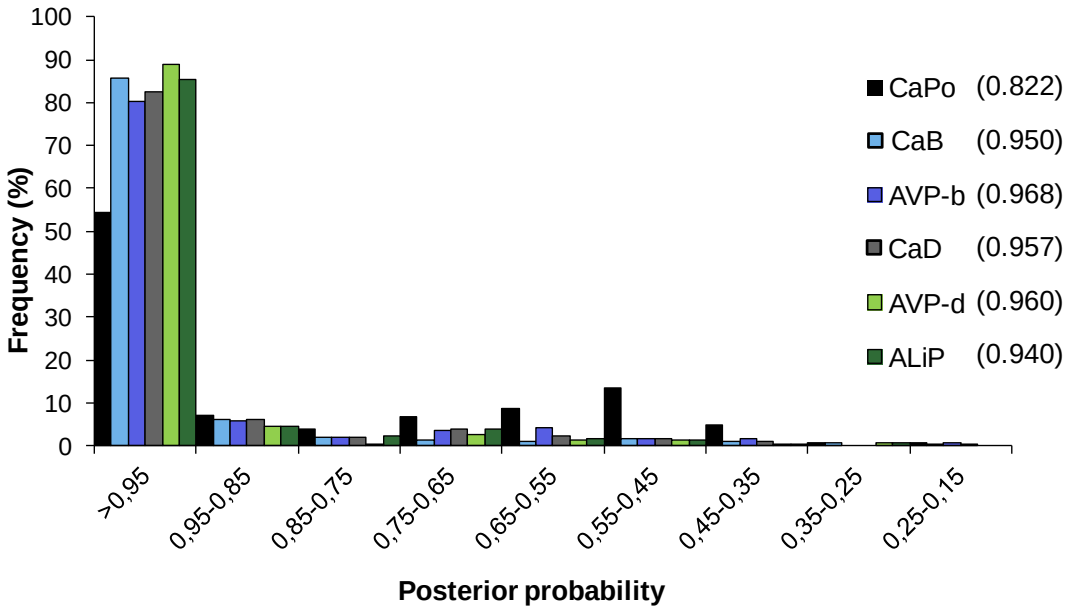

Fig. S1. Frequency distribution of amino acids with different posterior probabilities (i.e. the probability that a hypothesis is true after the data have been analyzed) for the six reconstructed ancestral sequences (**Fig. S2**) from the evolutionary lines B and D (**Fig. 1**). Most of the amino acids for each sequence have a posterior probability >0.95, showing the robustness of the sequence reconstruction. CaPo has a wider distribution, while for the other ancestors 80-90% of the predicted amino acids have a probability >0.95. The values in parenthesis represent the average probability for the complete sequences.

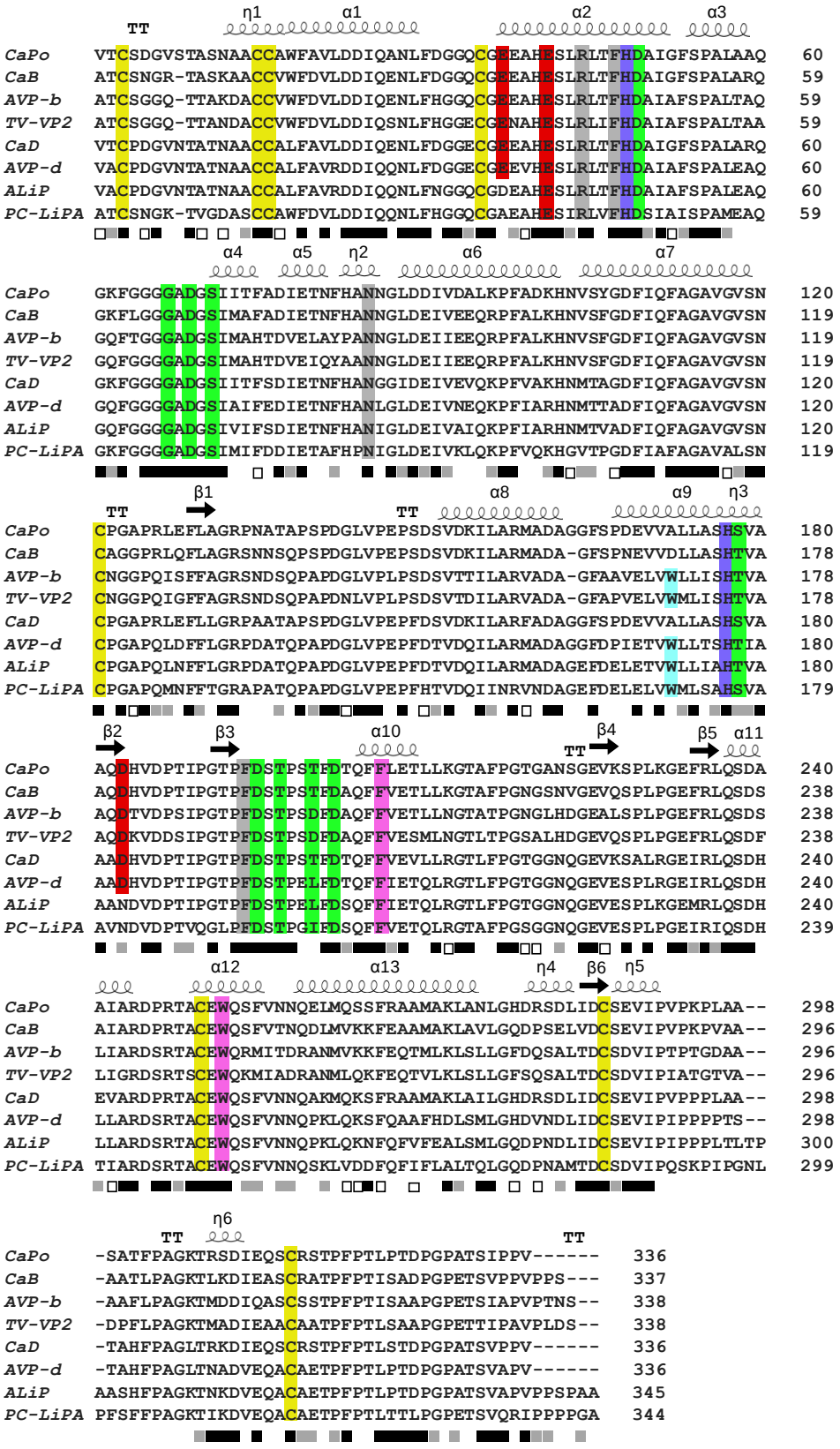

Fig. S2. Alignment of ancestral and extant (PC-LiPA and TV-VP2) sequences, with indication of: catalytic tryptophan (cyan), electron-transfer residues (pink), Mn^{2+}-binding site (red), active-site histidines (purple), other active-site residues (gray), Ca^{2+} ligands (green) and disulfide bonds (yellow) (15). Boxes (bottom) indicate full conservation of the same (black) or equivalent (gray) residues, and partial conservation (white). Secondary structure (top) includes: α, α-helices; η, 3_{10} helices; β, β-strands; and TT, strict β –turn.

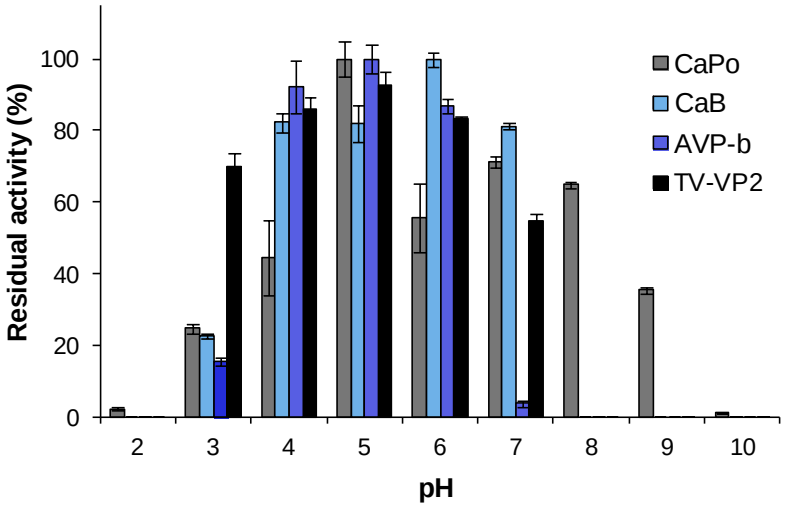

FIGURE S3. pH stability of line-B ancestral enzymes. Stability in the range of pH 2-10 was compared after 4-h incubation at 25ºC. Means and 95% confidence limits are shown.

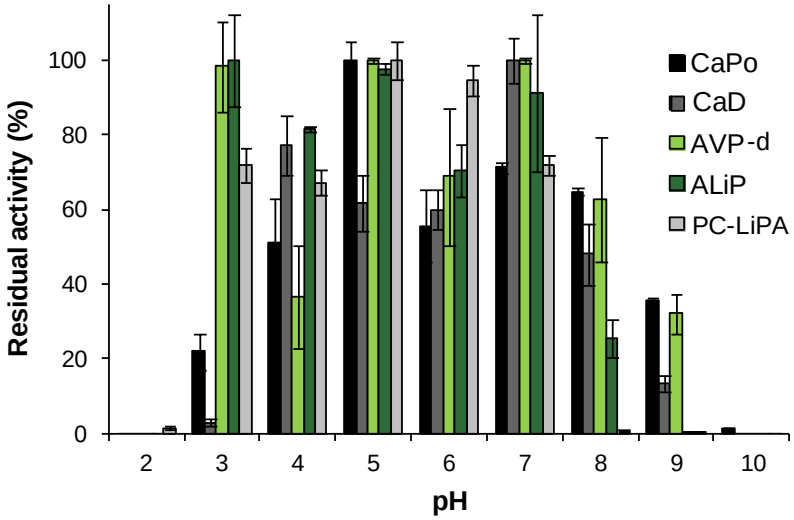

FIGURE S4. pH stability of line-D ancestral enzymes. Stability in the range of pH 2-10 was compared after 4-h incubation at 25ºC. Means and 95% confidence limits are shown. Adapted from Ayuso-Fernández et al. (16).

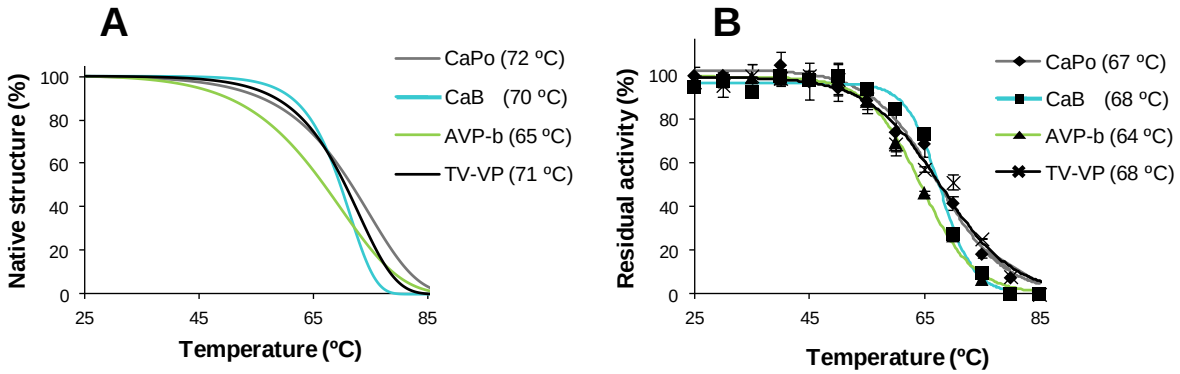

Fig. S5. Thermal stability of line-B ancestral peroxidases. **A)** Loss of secondary structure. **B)** Loss of activity. The T_m (**A**) and T_{50} (**B**) values are shown in the legends. Means and 95% confidence limits are shown in **B**.

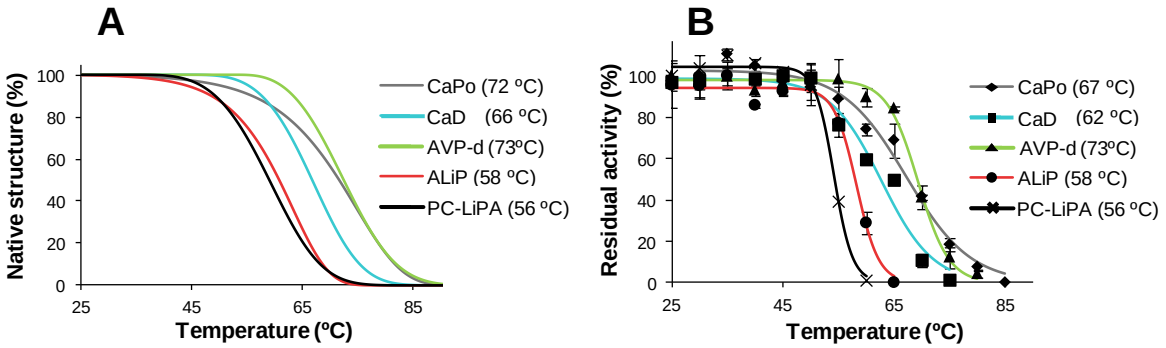

Fig. S6. Thermal stability of line-D ancestral peroxidases. **A)** Loss of secondary structure. **B)** Loss of activity. The T_m (**A**) and T_{50} (**B**) values are shown in the legends. Means and 95% confidence limits are shown in **B**. Adapted from Ayuso-Fernández et al. (16).

TABLE S1. Pairwise identity percentages between ancestral and extant (TV-VP2 and PC-LiPA) peroxidase sequences (the number of aligned residues are in parentheses)

	CaPo	CaB	AVP-b	TV-VP2	CaD	AVP-d	ALiP	PC-LiPA
CaPo	100 (336)	81 (275)	66 (223)	61 (208)	86 (289)	74 (248)	70 (242)	61 (209)
CaB		100 (337)	76 (257)	69 (233)	76 (259)	67 (226)	66 (227)	61 (211)
AVP-b			100 (338)	85 (288)	62 (211)	60 (205)	60 (207)	58 (199)
TV-VP2				100 (338)	59 (199)	59 (200)	57 (198)	56 (193)
CaD					100 (336)	80 (269)	75 (257)	61 (211)
AVP-d						100 (336)	87 (301)	66 (227)
ALiP							100 (345)	72 (249)
PC-LiPA								100 (344)

TABLE S2. Kinetic parameters - K_m (μM), k_{cat} (s^{-1}) and k_{cat}/K_m ($s^{-1}\cdot mM^{-1}$) - for oxidation of Mn^{2+}, DMP, ABTS, RB5 and VA by resurrected peroxidases from evolutionary lines B and D (**fig. 1**) and extant TV-VP2 and PC-LiPA.[a] See **Fig. 3** for graphical comparison of the peroxidase kinetic constants.

		Ancestral	Line-B (to VP)			Line-D (to LiP)[b]			
		CaPo[b]	CaB	AVP-b	TV-VP2	CaD	AVP-d	ALiP	PC-LiPA
Mn^{2+}	K_m	700 ± 48	132 ± 12	396 ± 82	3150 ± 550	275 ± 41	62 ± 10	-[c]	-
	k_{cat}	185 ± 3	121 ± 2	4 ± 0	11 ± 1	170 ± 6	106 ± 4	-	-
	k_{cat}/K_m	260±15	919 ± 73	9 ± 1	4 ± 1	617 ± 80	1710 ± 240	-	-
DMP[d] (low efficiency)	K_m	32900 ± 2700	635000 ± 27000	1400 ± 170	2300 ± 260	66800 ± 3800	32500 ± 12100	-	-
	k_{cat}	221 ± 9	404 ± 162	48 ± 1.7	130 ± 6	109 ± 4	31 ± 5	-	-
	k_{cat}/K_m	6.7 ± 0.3	0.6 ± 0.2	34.0 ± 3.0	56.0 ± 7.0	1.6 ± 0.0	1.0 ± 0.2	-	-
ABTS[d] (low efficiency)	K_m	3170 ± 270	1280 ± 350	314 ± 68	580 ± 80	1280 ± 350	2150 ± 420	-	-
	k_{cat}	539 ± 24	103 ± 10	163 ± 11	352 ± 13	103 ± 10	25 ± 2	-	-
	k_{cat}/K_m	170 ± 8	80 ± 10	500 ± 9	610 ± 70	80 ± 15	12 ± 1	-	-
DMP (high efficiency)	K_m	-	-	2.6 ± 0.6	8.9 ± 1.1	-	5.3 ± 1.1	34.0 ± 5.4	4.0 ± 0.1
	k_{cat}	-	-	4.4 ± 0.2	11.4 ± 0.4	-	4.5 ± 0.1	18.3 ± 0.7	6.9 ± 0.5
	k_{cat}/K_m	-	-	1700 ± 300	1300 ± 100	-	837 ± 162	537 ± 55	600 ± 36
ABTS (high efficiency)	K_m	-	-	48 ± 11	103 ± 36	-	5 ± 1	14 ± 4	21 ± 2
	k_{cat}	-	-	89 ± 8.7	128 ± 44	-	2 ± 0	13 ± 1	7 ± 0
	k_{cat}/K_m	-	-	1800 ± 300	2100 ± 300	-	400 ± 44	911 ± 212	300 ± 25
RB5	K_m	-	-	3.0 ± 0.4	2.8 ± 0.2	-	4.8 ± 0.8	12.6 ± 3.6	-
	k_{cat}	-	-	8.9 ± 0.5	8.6 ± 0.3	-	2.4 ± 0.2	5.4 ± 0.8	-
	k_{cat}/K_m	-	-	2900 ± 160	3100 ± 180	-	504 ± 50	428 ± 68	-
VA	K_m	-	-	10000 ± 100	24600 ± 200	-	299 ± 104	773 ± 155	79.3 ± 18
	k_{cat}	-	-	41 ± 1	172 ± 6.4	-	7 ± 1	21 ± 1	16 ± 1
	k_{cat}/K_m	-	-	4 ± 0	7 ± 0	-	24 ± 7	28 ± 5	205 ± 4

[a]Reactions at 25 °C in 0.1 M tartrate at optimal pH 5.0 (CaPo and CaD) or 5.5 (CaB, AVP-b, VP-d and TV-VP2) for Mn^{2+}, pH 3.5 (AVP-d), 3.0 (AVP-b, ALiP and PC-LiPA) or 2.0 (TV-VP2) for VA, pH 2 (CaPo and TV-VP2) or 3.0 (others) for DMP, pH 2 (TV-VP2), 3.0 (CaPo, CaB and AVP-b) or 3.5 (others) for ABTS, and pH 3 for RB5; and saturating H_2O_2 concentrations of 0.4 mM (CaPo, CaD, CaB, AVP-b, AVP-d and TV-VP2), 0.2 mM (ALiP) or 0.1 mM (PC-LiPA). [b]From Ayuso-Fernández et al. (16). [c]–, Absence of activityc. [d]Biphasic kinetics for DMP and ABTS oxidation by AVP-b, AVP-d and TV-VP2 enabled calculation of two sets of constants assigned to two catalytic sites, as reported for *P. eryngii* VP (17). Means and 95% confidence limits are provided.

Supporting References

1. Binder, M, Justo, A, Riley, R, Salamov, A, Lopez-Giraldez, F *et al.* (2013) Phylogenetic and phylogenomic overview of the Polyporales. *Mycologia* 105: 1350-1373.
2. Fernández-Fueyo, E, Ruiz-Dueñas, FJ, Ferreira, P, Floudas, D, Hibbett, DS *et al.* (2012) Comparative genomics of *Ceriporiopisis subvermispora* and *Phanerochaete chrysosporium* provide insight into selective ligninolysis. *Proc Natl Acad Sci USA* 109: 5458-5463.
3. Floudas, D, Binder, M, Riley, R, Barry, K, Blanchette, RA *et al.* (2012) The Paleozoic origin of enzymatic lignin decomposition reconstructed from 31 fungal genomes. *Science* 336: 1715-1719.
4. Ohm, RA, Riley, R, Salamov, A, Min, B, Choi, IG *et al.* (2014) Genomics of wood-degrading fungi. *Fungal Genet Biol* 72: 82-90.
5. Martinez, D, Challacombe, J, Morgenstern, I, Hibbett, DS, Schmoll, M *et al.* (2009) Genome, transcriptome, and secretome analysis of wood decay fungus *Postia placenta* supports unique mechanisms of lignocellulose conversion. *Proc Natl Acad Sci USA* 106: 1954-1959.
6. Kumar, S, Stecher, G, Tamura, K (2016) MEGA7: Molecular evolutionary genetics analysis version 7.0 for bigger datasets. *Mol Biol Evol* 33: 1870-1874.
7. Abascal, F, Zardoya, R, Posada, D (2005) ProtTest: selection of best-fit models of protein evolution. *Bioinformatics* 21: 2104-2105.
8. Stamatakis, A, Hoover, P, Rougemont, J (2008) A rapid bootstrap algorithm for the RAxML web servers. *Syst Biol* 57: 758-771.
9. Whelan, S, Goldman, N (2001) A general empirical model of protein evolution derived from multiple protein families using a maximum-likelihood approach. *Mol Biol Evol* 18: 691-699.
10. Yang, ZH (2007) PAML 4: Phylogenetic analysis by maximum likelihood. *Mol Biol Evol* 24: 1586-1591.
11. Biasini, M, Bienert, S, Waterhouse, A, Arnold, K, Studer, G *et al.* (2014) SWISS-MODEL: Modelling protein tertiary and quaternary structure using evolutionary information. *Nucleic Acids Res* 42: W252-W258.
12. Guex, N, Peitsch, MC, Schwede, T (2009) Automated comparative protein structure modeling with SWISS-MODEL and Swiss-PdbViewer: A historical perspective. *Electrophoresis* 30: S162-S173.
13. Pérez-Boada, M, Doyle, WA, Ruiz-Dueñas, FJ, Martínez, MJ, Martínez, AT *et al.* (2002) Expression of *Pleurotus eryngii* versatile peroxidase in *Escherichia coli* and optimisation of *in vitro* folding. *Enzyme Microb Technol* 30: 518-524.
14. Doyle, WA, Smith, AT (1996) Expression of lignin peroxidase H8 in *Escherichia coli*: Folding and activation of the recombinant enzyme with Ca^{2+} and haem. *Biochem J* 315: 15-19.
15. Ruiz-Dueñas, FJ, Morales, M, García, E, Miki, Y, Martínez, MJ *et al.* (2009) Substrate oxidation sites in versatile peroxidase and other basidiomycete peroxidases. *J Exp Bot* 60: 441-452.
16. Ayuso-Fernández, I, Martínez, AT, Ruiz-Dueñas, FJ (2017) Experimental recreation of the evolution of lignin degrading enzymes from the Jurassic to date. *Biotechnol Biofuels* 10:67.
17. Morales, M, Mate, MJ, Romero, A, Martínez, MJ, Martínez, AT *et al.* (2012) Two oxidation sites for low redox-potential substrates: A directed mutagenesis, kinetic and crystallographic study on *Pleurotus eryngii* versatile peroxidase. *J Biol Chem* 287: 41053-41067.